iScience

Article

Supplementary motor area in speech initiation: A large-scale intracranial EEG evaluation of stereotyped word articulation

Graphical abstract

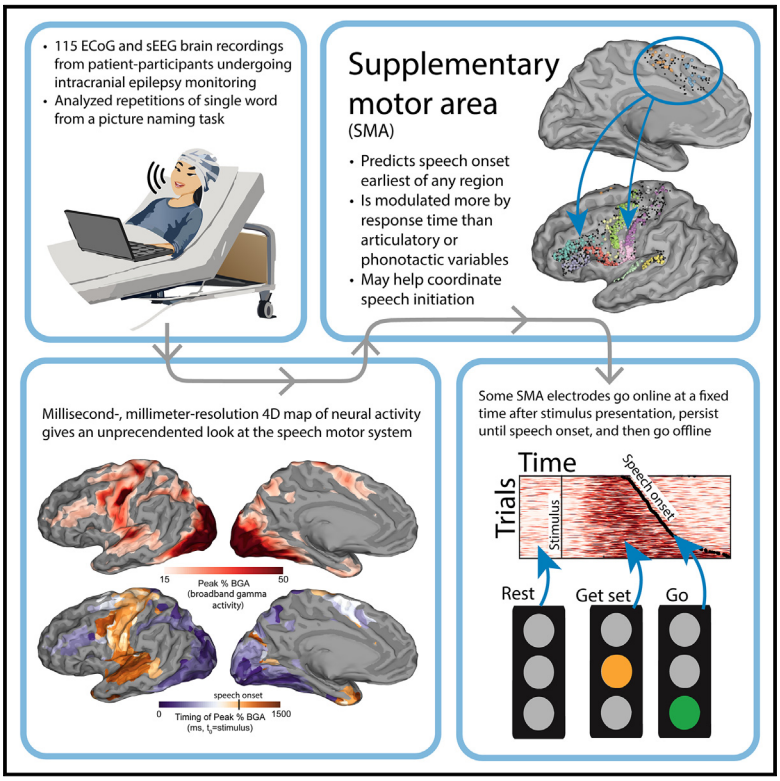

Highlights

- 4D millisecond-resolution brain map of word articulation from 115 iEEG recordings
- SMA and preSMA predict speech onset as early as any region
- Some SMA and preSMA electrodes time-lock to both stimulus onset and speech onset

Authors

Latané Bullock, Kiefer J. Forseth, Oscar Woolnough, Patrick S. Rollo, Nitin Tandon

Correspondence

nitin.tandon@uth.tmc.edu

In brief

Neuroscience; Sensory neuroscience

Bullock et al., 2025, iScience *28*, 111531
January 17, 2025
https://doi.org/10.1016/j.isci.2024.111531

CellPress

iScience

CellPress
OPEN ACCESS

Article

Supplementary motor area in speech initiation: A large-scale intracranial EEG evaluation of stereotyped word articulation

Latané Bullock,[1,2,5] Kiefer J. Forseth,[1,2,3,5] Oscar Woolnough,[1,2] Patrick S. Rollo,[1,2] and Nitin Tandon[1,2,4,6,*]
[1]Vivian L. Smith Department of Neurosurgery, McGovern Medical School at UT Health Houston, Houston, TX 77030, United States of America
[2]Texas Institute for Restorative Neurotechnologies, University of Texas Health Science Center at Houston, Houston, TX 77030, United States of America
[3]Department of Neurological Surgery, University of California, San Diego, La Jolla, CA 92093, United States of America
[4]Memorial Hermann Hospital, Texas Medical Center, Houston, TX 77030, United States of America
[5]These authors contributed equally
[6]Lead contact
*Correspondence: nitin.tandon@uth.tmc.edu
https://doi.org/10.1016/j.isci.2024.111531

SUMMARY

Speech production engages a distributed network of cortical and subcortical brain regions. The supplementary motor area (SMA) has long been thought to be a key hub in coordinating across these regions to initiate voluntary movements, including speech. We analyzed direct intracranial recordings from 115 patients with epilepsy as they articulated a single word in a subset of trials from a picture-naming task. We aimed to characterize the temporal dynamics of SMA relative to other cortical regions. SMA and preSMA were among the first regions to activate after cue onset, peaked in activity before articulation onset, and were the earliest regions to predict trial-to-trial response time. Neural activity at single electrodes in SMA and preSMA was closely associated with speech initiation; activity began at a highly predictable time after stimulus onset and extended until speech onset for any given trial. Our results support the idea that SMA is a key node in the speech initiation network.

INTRODUCTION

Initiation of voluntary movement requires coordinated activity between brain regions specifying movement context and contingencies and brain regions executing motor plans and monitoring their sensory consequences. The supplementary motor area (SMA) has long been proposed as a critical node in coordinating these processes across many voluntary movements,[1] including propositional speech in humans.[2–5] SMA stimulation can result in speech arrest,[6] and SMA lesions may result in impaired propositional speech.[4,7] Yet, its contribution to speech production remains poorly characterized compared to lateral speech areas, such as ventral sensorimotor cortex (vSMC) and premotor cortex, due to methodological limitations. While fMRI has been used to probe SMA's role in speech,[2,8–11] its temporal resolution precludes conclusions on the timescale necessary for speech (tens of milliseconds). Temporally resolved non-invasive methodologies also present challenges for studying SMA and speech; signal quality in medial areas is low in magnetoencephalography,[12] and event-related potentials in scalp electroencephalography (EEG) do not localize to a specific area of cortex.[1,13] Finally, while human intracranial recordings have been key to elucidating the cortical control of speech articulators[14–16] and speech initiation,[17–20] they have mostly been limited to lateral frontal and rolandic gyral cortex due to clinical considerations in epilepsy surgery.

Single-unit recordings and local field potentials (LFPs) from non-human primates reveal that SMA and preSMA play an important role in initiating[21] and sequencing[22,23] limb movements. SMA has robust structural connectivity via the frontal aslant tract to ventral premotor and sensorimotor speech cortices, concordant with a putative role for the SMA initiating a "go" signal or "igniting" speech motor output.[24,25] Some current models of speech production thus hypothesize that the cascade of speech motor areas begins with coordination between basal ganglia and SMA,[26] but direct, temporally precise evidence for this in humans is lacking.

We utilized fine-grained human intracranial EEG (iEEG) recordings to analyze the activity of the SMA relative to the activation of the speech motor network via large-scale intracranial recordings (n = 115 patients, 125 implants) in a picture-naming task.[27] Penetrating depth electrodes covered the broad articulation network, including the medial frontal cortex (i.e., preSMA and SMA). Further, we achieve unprecedented temporal precision by analyzing the repetition of a single stereotyped word—"scrambled"—that participants produced scores of times in response to a jumbled image (8,078 total trials). This enabled the investigation of trial-by-trial variations in response time (RT), without the confound of varying phonological or semantic features.

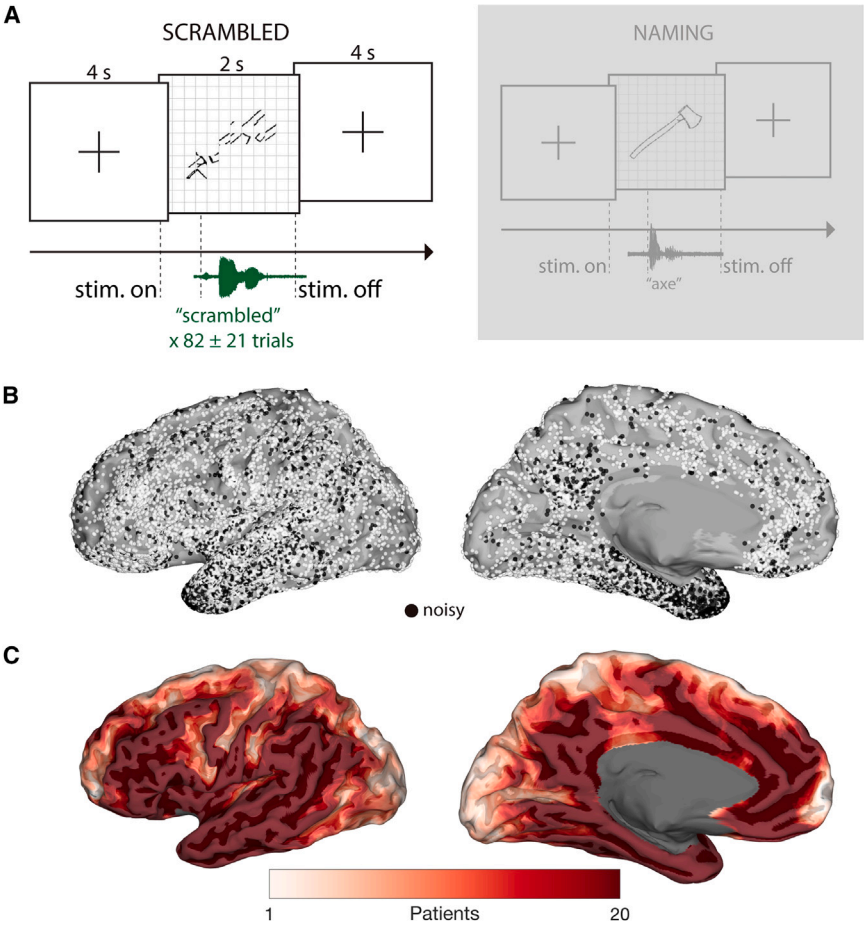

Figure 1. Experimental design and cortical coverage

(A) Patients articulated "scrambled" in response to an incoherent image in one-third of trials (left) or named common objects in two-thirds of trials (right, gray overlay).

(B) Coverage of language-dominant cortex with intracranial EEG. Implanted electrodes registered to a standard semi-inflated pial surface. White spheres indicate clean electrodes used in subsequent analyses. Black spheres indicate electrodes excluded due to noise.

(C) Cohort coverage map on semi-inflated surface.

RESULTS

Overview

115 patients with epilepsy completed a picture-naming task from the Snodgrass and Vanderwart[28] picture set with stereo-EEG (sEEG) (n = 86 implants) or subdural grid electrode (SDE) (n = 39 implants) recordings (Figure 1A). Electrodes extensively covered the language-dominant hemisphere in both lateral areas and medial areas (Figures 1B and 1C). In this study, we focus on the control condition of the picture-naming task, in which subjects responded to incoherent images with the word "scrambled."[27] 82 ± 21 (mean ± SD) scrambled trials were presented per subject. Across the cohort, the word "scrambled" was produced 10,788 times.

Behavioral analysis

Mean accuracy across the cohort during the scrambled trials was 98% ± 4% (range: 67%–100%). Mean RT across the cohort was 1,139 ± 298 ms. sEEG subjects responded, on average, 214 ms faster than SDE subjects (unpaired t test, t(123) = 4.42, $p < 0.001$, 95% confidence interval [CI] 118 to 310 ms), likely as patients with SDEs generally require a greater dosage of narcotics after surgery[29,30] (Figures 2A and 2B). The mean duration of articulation of "scrambled" was 638 ± 110 ms.

We were interested in the articulatory variability of this single stereotyped word "scrambled" within and across subjects. Using the Montreal Forced Aligner,[32] we identified approximate phoneme boundaries for each "scrambled" production in subjects with sufficiently clear audio recordings (n = 40 subjects) (Figures 2C and 2D). Articulatory variability of each phoneme in "scrambled" accumulated variability of preceding phonemes; the first phoneme's offset standard deviation was 59 ms relative to speech onset, while the last phoneme's offset standard deviation was 131 ms relative to speech onset. It is worth noting two aspects of "scrambled" articulation in the dataset. First, the second syllable was often greatly reduced, such that the spectral energy in the first syllable exceeded that of the second.[33] Second, we observed variability in the presence of the word-final phoneme/d/. Some subjects articulated "scrambled" while others articulated "scramble."

4D global mean broadband gamma power dynamics

To inspect cortical activity across the cohort during stereotyped word articulation, we utilized a surface-based mixed-effects multilevel analysis (SB-MEMA) technique that reliably co-registers activity across subjects onto a population standard surface, robustly accounts for trial and subject outliers, and infers activity at every point on the cortical surface.[34,35] We used broadband gamma activity (BGA, 70–150 Hz) at each electrode as it is associated with both local spiking activity[36] and blood-oxygen-level-dependent response.[37] Repeating SB-MEMA analyses in short, overlapping windows (10 ms steps, 150 ms duration) resulted in a 4D representation of cortical dynamics during the articulation of "scrambled" (Figure 3; Videos S1 and S2). We performed this analysis time-locked to speech onset (Video S1) and time-locked to stimulus onset (Video S2).

As expected, occipital cortex was the earliest region in both hemispheres to activate in response to the visual cue. Around 200 ms after stimulus onset, SMA, precentral sulcus, and posterior inferior frontal sulcus (IFS; Video S2) became active. A short

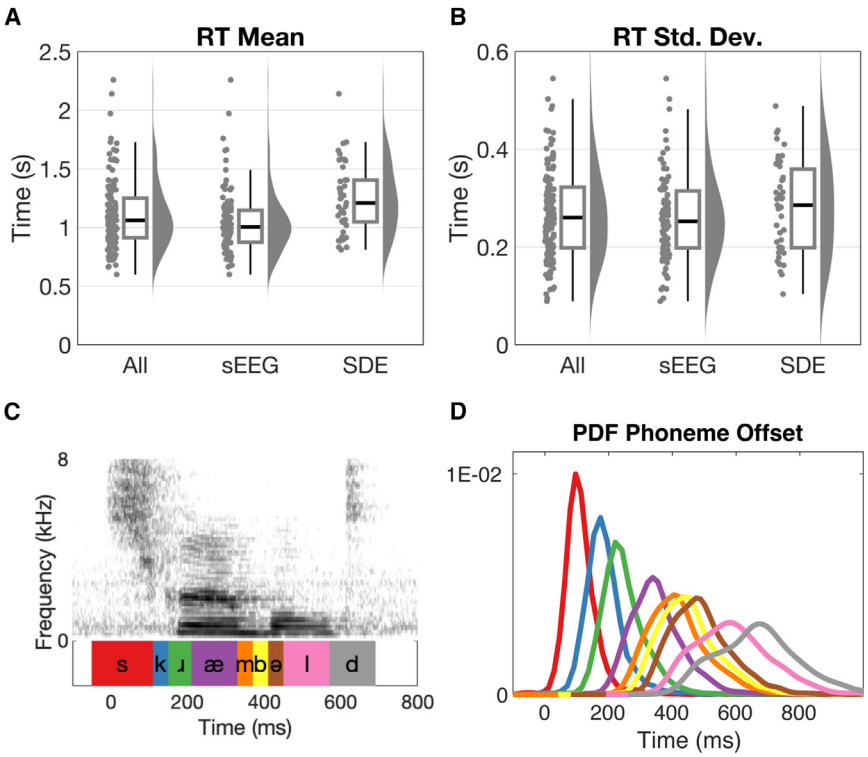

Figure 2. "Scrambled" response time and articulatory variability

(A and B) Mean (A) and standard deviation (B) of response time (RT) distributions for all subjects and separately for sEEG implants only, and SDE only. Each data point represents the mean or standard deviation of RT for a single subject. Box-and-whisker plots indicate median, upper and lower quartiles, and extent of outliers. Half-violin plots depict probability density estimates for each dataset using default parameters of the ksdensity() MATLAB function.[31]

(C) Spectrogram and corresponding phoneme boundaries identified by the Montreal Forced Aligner (McAuliffe et al., 2017) for one "scrambled" production. Time-zero is word onset as manually labeled by inspecting the spectrogram.

(D) Probability distribution function of phoneme offsets color-coded from phonemes in (C). These distributions were generated from a subset of subjects (n = 40) with sufficiently clear audio for automated phonemic transcription.

time later (~250 ms), the anterior IFS and superior frontal sulcus became active. At 400 ms, premotor, primary motor, and sensorimotor regions became engaged and remained active for the duration of the articulation of the word. When visualizing timing of peak BGA activity (Figure 3B), the SMA's activity is partially coincident with IFS (purple) and precedes subsequent motor and premotor areas (orange).

We did not observe a somatosensory articulatory map emerge at cohort level in ventral precentral gyrus and postcentral gyrus (postCG) despite the stereotyped nature of the articulation; in the population map, ventral and dorsal pre- and postcentral gyri engaged simultaneously. Given the existence of articulator maps in single-subject and few-subject studies,[38] the absence of a population map may be the result of inter-subject anatomical and functional variability.

BGA in articulation regions of interest

We next sought to compare SMA and preSMA activation time courses to that of other speech motor regions. Using the global activation maps (Figure 3; Video S1), we probed 12 anatomical-functional regions of interest (ROIs) in the language-dominant hemisphere (Figure 4A; see STAR Methods for ROI definitions). In addition to the supra-sylvian speech production network, we included Heschl's gyrus and planum temporale given their proposed role in articulation monitoring and error detection.[39,40] ROI trial-averaged time series traces revealed a cascade of activations with varying onsets of activation, rates of activation, magnitude of activation, and duration of activation (Figure 4B).

Along with preSMA and SMA, IFS was among the earliest regions to engage and to peak. IFS diverged from medial frontal activity; however, in that, its activity was sustained beyond speech onset. PreSMA and SMA activity quickly declined after peaking, while IFS activity was sustained throughout articulation. IFS was also unique among ROIs in its biphasic profile; it had a local maximum 250 ms before speech onset and, interestingly, another around 400 ms after speech onset (Figure 4B, right). Some regions, like preSMA, had quick-rise (~300 ms) activation profiles while others, like postCG, ramped up slower throughout 500+ ms (Figure 4B). Activity in precentral gyrus, subcentral gyrus, and postCG peaked just after articulation onset, and these sites remained active even after articulation offset.

A subset of pars opercularis and pars triangularis electrodes were task activated (Figure 4A). They were, however, low in activation amplitude (Figure 4B) and inconsistent enough to be absent in the MEMA analysis (Figure 3), in line with recent evidence suggesting that inferior frontal gyrus plays only a minor role in speech articulation.[41–44]

In addition to these trial-averaged analyses, we bootstrapped BGA traces within each region to estimate 95% confidence intervals of BGA timing features: time to peak BGA amplitude and the time to the first time point at which BGA was greater than baseline (Table 1). Median (95% CI) time to peak BGA relative to stimulus onset was 540 (460–600) ms for preSMA and 590 (530–650) ms for SMA. Activity in preSMA and SMA peaked prior to speech onset; median (95% CI) time to peak BGA relative to speech onset was −240 ms (−330 to −190) for preSMA and −170 ms (−230 to −150) for SMA. IFS and preSMA "time to peak amplitude" confidence intervals intersected; we cannot therefore make any statements about their relative timing. IFS and SMA, however, had non-overlapping intervals, providing evidence that IFS time to peak precedes SMA time to peak.

Spectrograms were calculated for each of the ROIs to inspect full-spectrum changes relative to baseline (Figure 4C). In all

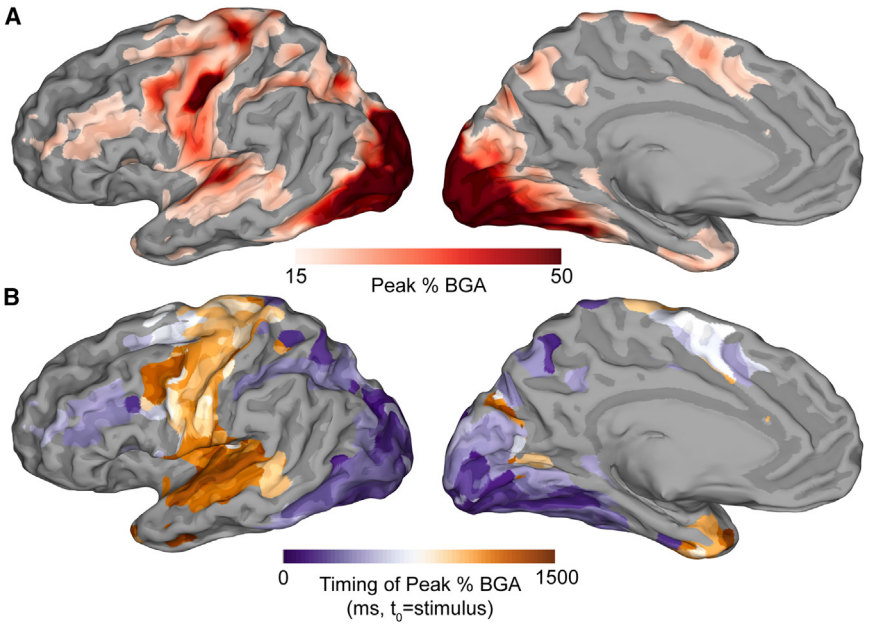

Figure 3. Cohort broadband gamma activity inferred with surface-based mixed-effects multilevel analysis

(A) Peak mean BGA percentage thresholded at 15% increase relative to baseline.

(B) Timing of peak BGA with respect to stimulus onset. Refer to Video S1 for the full 4D rendition in both hemispheres.

ROIs, BGA increases were expectedly accompanied by beta decreases. PreSMA beta decreases were smaller than other regions when scaled by BGA increases.

SMA activity predicts trial RT

To further probe the role of SMA in speech initiation, we asked how does single-trial BGA in SMA and preSMA contribute to the prediction of RT? The highly stereotyped nature of the "scrambled" articulations eliminated confounds of other linguistic variables. We ran linear mixed-effects models in each ROI, for each 10 ms interval, modeling BGA as a function of RT (fixed effect) and electrode, nested within subject (random effects). We found neural activity in SMA was modulated by RT early—just 270 ms after stimulus onset—and that preSMA and IFS followed SMA about 50 ms later (Figure 4D). Activity in pars opercularis, pars triangularis, and precentral sulcus did not co-vary with RT despite early activation (Figure 4D). Speech monitoring regions, Heschl's gyrus and planum temporale, showed initial significance around the earliest articulation onsets given that they are time-locked to articulation.

Drivers of activation in SMA

The aforementioned analyses highlighted the early role of SMA and preSMA in the cascade of regions leading up to articulation. We did not observe meaningful differences between SMA and preSMA in previous analyses, so we included electrodes from both regions in subsequent analyses. We next inspected individual electrodes in these regions more closely to characterize their patterns of activation (Figure 5). Electrodes displayed variable responses across the region (Figures 5A and 5B), but a stereotyped response was evident (Figures 5C and 5D). Electrodes activated at a predictable time after stimulus onset and disengaged at a predictable time prior to speech onset or at speech onset (Figure 5D). Given the homogeneity of the "scrambled" trials, we attributed this trial-to-trial variability as primarily indexing the readiness of the speech production system to articulate. If this reasoning were true, coherent trials in which the participant named an object (e.g., apple) should follow the same pattern. Indeed, in coherent trials (which had longer RT than "scrambled" trials), electrodes activated at the same time as in "scrambled" articulation, but then sustained activation until speech onset (Figure 5D, red). Thus, BGA was prolonged in trials with greater RT.

To assess if these RT-driven electrodes are modulated by other behavioral correlates (e.g., articulatory complexity), we tested the sensitivity of BGA in coherent trials from the picture-naming task at the group level with linear mixed-effects modeling (Figure 6). We modeled BGA in the 300 to 600 ms window post-stimulus as a function RT, number of syllables, word frequency, and phonological neighborhood. We were thus able to test how RT (relative to other behavioral predictors) contributes to BGA in a held-out dataset. The linear mixed-effects model (300–600 ms post-stimulus, $r^2 = 0.58$) showed that BGA was significantly modulated by RT ($t(5627) = -4.0$, $p < 0.001$, 95% CI −35 to −12) and word frequency ($t(5627) = -2.5$, $p = 0.012$, 95% CI −29 to −4). Number of syllables ($t(5627) = -0.9$, $p = 0.35$, 95% CI −16 to 6) and phonological neighborhood density ($t(5627) = 1.1$, $p = 0.25$, 95% CI −4 to −14) did not significantly modulate BGA in SMA.

DISCUSSION

Speech initiation requires coordination across multiple cortical regions. The SMA, among other roles in speech,[45] may relay a "go" signal from the basal ganglia when high-level language areas and low-level sensorimotor areas are all ready to initiate a speech sequence. Here, we analyzed intracranial recordings as subjects repeatedly (~80 times) articulated the word "scrambled" during a picture-naming task. We found evidence largely concordant with the idea that the preSMA-SMA complex is a key node in the brain's speech initiation network.

From a comprehensive 4D cortical atlas, we extracted a cohort to show that the preSMA and SMA, along with IFS, are the earliest cortical speech regions to activate during cued, stereotyped word production (Figures 3 and 4B; Videos S1 and S2). Additionally, activity was predictive of articulation onset at the single-trial level, and again it was one of the earliest regions to do so (Figure 4D). Finally, we uncovered a stereotypical BGA response in preSMA and SMA during articulation preparation, with some electrodes showing remarkably consistent time-locking to intent-to-speak

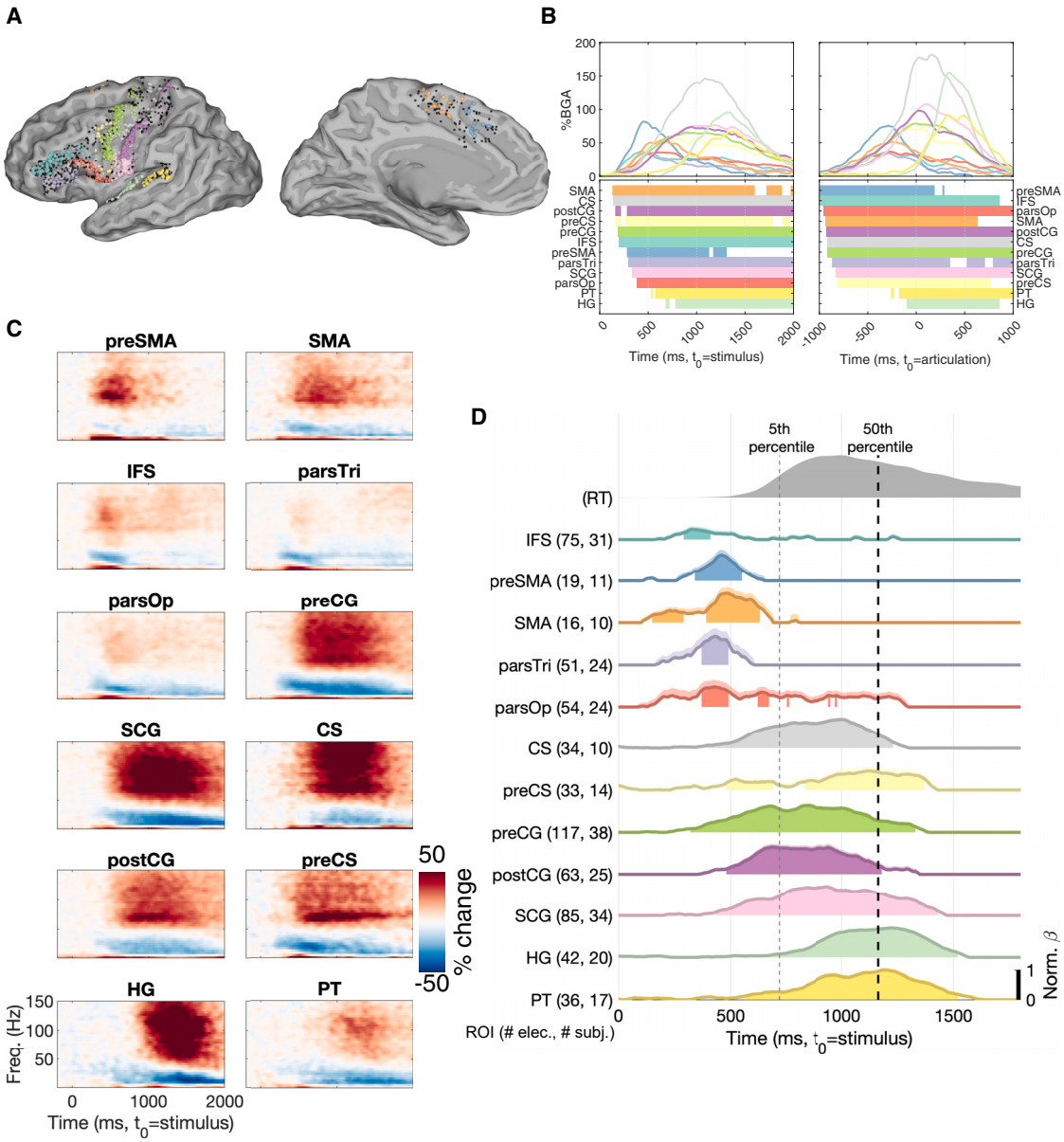

Figure 4. Language-dominant hemisphere broadband gamma activity in regions of interest: trial-averaged and single-trial response time correlation

(A) Regions of interest delineation on the standard cortical surface. Every electrode localized to the region is shown. Active electrodes are colored according to region. See (B) and (D) for color code and region names. Inactive electrodes are depicted in black.

(B) Average BGA traces for each ROI time-locked to stimulus (left) and to speech onset (right). Periods of significant activation above baseline (Wilcoxon signed-rank, FDR-corrected, $q < 0.05$) are indicated in the bottom panel. ROIs are sorted by onset of significance.

(C) ROI-averaged spectrograms time-locked to stimulus onset in the 12 ROIs.

(D) Linear mixed-effects (LME) modeling of BGA as a function of response time (RT) in each ROI. LME beta values were half-wave rectified—interpretable as positive beta values indicating greater BGA in faster RT trials. The distribution of cohort RTs is plotted above in gray, with the dashed lines denoting the fifth percentile and median RTs. Shaded area extending upward from the beta curve denotes standard error. Time points which reach significance (FDR-corrected, $q < 0.05$) are filled in under the curve. Abbreviations: IFS, inferior frontal sulcus; preCS, precentral sulcus; parsTri, pars triangularis; parsOp, pars opercularis; preSMA, pre-supplementary motor area; SMA, supplementary motor area-proper; preCG, precentral gyrus; SCG, subcentral gyrus; CS, central sulcus; postCG, postcentral gyrus; HG, Heschl's gyrus; PT, planum temporale.

and articulation onset (Figures 5C and 5D). preSMA and SMA electrodes were modulated almost exclusively by RT, a conclusion supported by the fact that (1) BGA was prolonged in trials with longer RT (Figure 5) and (2) other factors, like articulatory complexity, accounted for an insubstantial portion of BGA variance (Figure 6). This is in line with the idea that preSMA and

Table 1. Timing features of BGA traces across regions of interest

Region	Time to peak Amp (ms)	Time to first Amp > baseline (ms)
IFS	460 (450–520)	120 (90–130)
preSMA	540 (460–600)	160 (130–180)
SMA	590 (530–650)	140 (90–170)
parsTri	670 (580–720)	240 (51.25–270)
parsOp	750 (640–860)	130 (20–170)
CS	1,030 (990–1,060)	130 (80–208.75)
preCS	1,040 (980–1,310)	100 (40–145.25)
preCG	1,100 (970–1,160)	20 (10–120)
postCG	1,130 (1,070–1,240)	160 (70–210)
SCG	1,220 (1,190–1,370)	250 (10–320)
HG	1,360 (1,310–1,400)	690 (90–760)
PT	1,360 (1,280–1,430)	50 (10–120)

Timing features within each ROI were calculated by bootstrapping trial traces (see STAR Methods). Times are reported as "median (95% confidence interval)" with respect to stimulus onset. Time to peak Amp is the time point at which BGA reached maximum. Time to first Amp > baseline is when a region first activated with respect to baseline. ROIs are sorted by time to peak Amp. ROI abbreviations are as enumerated in Figure 4 legend.

SMA lie at the heart of the speech initiation circuit.[26] Our results do not directly support the idea that preSMA and SMA initiate linguistic units smaller than words (like syllables or phonemes), nor the idea that preSMA and SMA encode indices of articulatory complexity like syllable count or phonological neighborhood; however, these factors may modulate the supplementary motor cortex activity at smaller spatial scales than LFPs.[22]

Previous non-invasive[9] and invasive[46,47] studies have yielded conflicting results regarding whether SMA is primarily involved in pre-movement planning window *prior* to speech onset or primarily engaged *during* speech execution, or both. Our results primarily support the preparation-window thesis; activity at the group (Figure 4) and single-electrode level (Figures 5D and 5E) was largely constrained to the pre-speech window. There were, however, some electrodes which revealed execution-window activity (that is, *during* speech) (Figure 5A).

The role of SMA in speech initiation and timing

Penfield and Welch[5] established a causal role of the SMA in speech production with electrical cortical stimulation. Since then, the SMA has been further described as the site of "speech motor emission"[3] and of speech gesture sequencing.[48] EEG studies revealed that SMA is the earliest region to peak in neural activity during speech production and that SMA activity peaks just prior to speech onset.[49,50] While the SMA is recognized in some current models of speech production,[26] it is absent in others.[40,51] Recent evidence of SMA in non-human primates has supported the idea that the SMA area mediates motor gesture release. SMA maintains both internal (perceptual) and external (motor) rhythms in rhesus monkeys, suggesting that SMA is not only responsible for voluntary motor initiation but also for managing rhythmic motor commands.[52–54] Speech production, pseudo-rhythmic itself,[55,56] may recruit SMA for monitoring and managing the release of speech motor commands at regular intervals.[45] Our results corroborate the motor-release hypothesis for a single word but are agnostic to the question of phrase or discourse-level speech.

The DIVA/GODIVA computational model of speech production has developed to include the SMA and preSMA to account for SMA's reliable activation in even simple speech utterances and preSMA's role in speech sequencing.[26,57,58] GODIVA hypothesizes that preSMA and IFS instantiate a "cognitive context" that holds context in memory until the appropriate motor gesture has been produced, at which point preSMA sends an initiation signal to SMA. SMA, in turn, interfaces with basal ganglia to "release" the planned speech acts.[26,45] Our results suggest that, at the LFP level, words are the units of release for the region, rather than the syllables or phonemes within the word; we observed activity prior to speech onset only, rather than peaks of activity for each syllable or phoneme (Figure 5). Our results begin to clarify the nature of SMA's "release" of motor commands in the model. Previously, various possibilities existed for how this was achieved. For example, SMA could activate just prior to speech onset—independent of reaction time—if it were receiving a transient "go" signal from the basal ganglia.[59] Our results, however, suggest that the stereotypical SMA response is time-locked to both intention to speak (cue onset) and the release of the motor command (speech onset). Thus, it is the *silencing* of BGA in SMA that indexes with the release of motor commands at the LFP spatial scale.

SMA activity offset coincided with vPMC and M1 activity onset at speech onset. This, along with existing literature, is in line with that the SMA coordinates the concerted activation of vPMC and M1. But future research establishing a causal connection will need to elaborate on this speculation.

SMA and preSMA are known to have different cytoarchitectonic compositions,[60] functional connectivity,[60] and structural connectivity.[25] These differences are, however, manifested in a slow gradient fashion across the medial premotor cortex rather than respecting microanatomical landmarks.[2,61] Our analyses did not reveal striking differences between the two regions. Denser coverage in future iEEG studies may reveal patterns we did not have the sensitivity for in the current study. Different task demands, such as sentence articulation or a task requiring

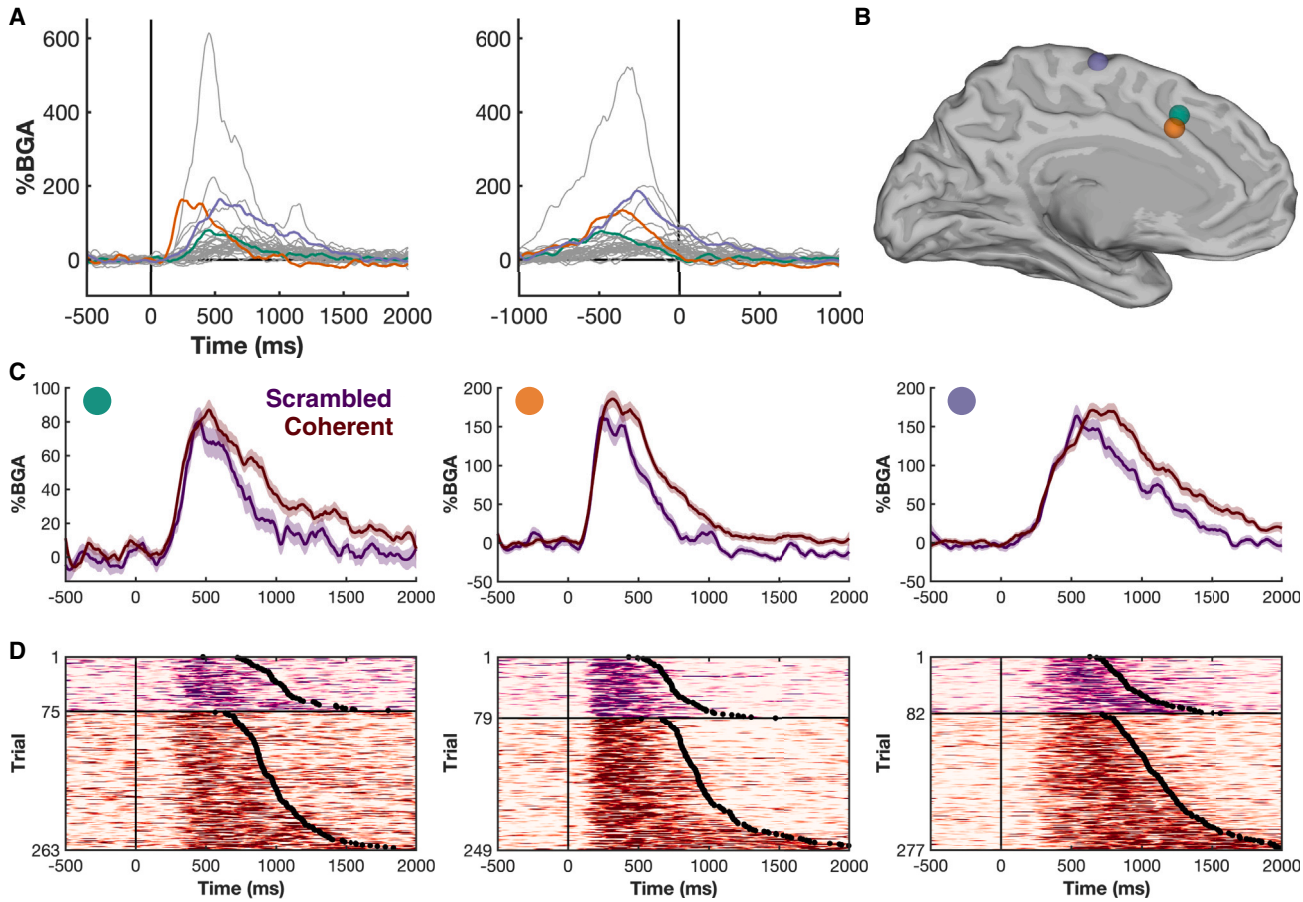

Figure 5. Functional broadband gamma activity in SMA for both scrambled and coherent picture naming conditions

(A) Mean BGA traces for scrambled trials for each electrode in the SMA or preSMA ROIs, locked to stimulus onset (left) or articulation onset (right), highlighting exemplar electrodes used for further analysis.

(B–D) Exemplar electrodes from three different subjects: (B) locations in group-normalized space, (C) mean BGA traces (± SE) for coherent (red) and scrambled (purple) trials, and (D) trial-by-trial raster plots of BGA for coherent (red) and scrambled (purple) trials, sorted by trial RT.

prosodic control, might also help disentangle these regions further.

SMA in pathological speech

The SMA has been implicated in a number of speech production disorders: namely, stuttering,[59,62,63] apraxia of speech,[64,65] SMA syndrome,[66,67] and idiosyncratic aphasias.[68] SMA is often understood as a messenger node relaying sensorimotor context and timing information during production from basal ganglia and thalamus to appropriate cortical areas.[69] Our results corroborate this hypothesis by providing evidence for the SMA's role in speech initiation.

The high recovery rate of SMA syndrome[67,70,71] and SMA lesions[66] suggests that while SMA is indispensable for speech initiation in a neurologically intact brain, the initiation network is degenerate,[72] with compensatory mechanisms readily available. The left and right SMAs may complement each other to a greater degree than other speech motor nodes, as SMA syndrome recovery is associated with increased right SMA connectivity with lateral speech regions.[67,73]

SMA in brain-computer interfaces

We suggest that future brain-computer interfaces can leverage SMA to index timing of voluntary speech acts. SMA was the earliest predictor of speech onset. 250 ms after stimulus presentation, SMA activity significantly predicts RT. vSMC, which has been used to detect speech onset, becomes predictive more than 100 ms later, at 380 ms (Figure 2). In addition to offering an earlier prediction of voluntary speech acts than vSMC, SMA is a better speech detector in that (1) it may be more active than vSMC during imagined, unexecuted speech[74,75] and (2) it houses single-site predictors of speech onset, which would alternatively have to be derived from the activity across many electrodes in vSMC.[76]

Other early-activation regions: IFS

Other speech network nodes were consistently active early in the pre-articulation window. Most notably, IFS activated and peaked at times on par with the SMA complex (Figure 4B, Table 1, and Video S1). In contrast to SMA complex, however, IFS is likely not critical in speech initiation based on our results here as

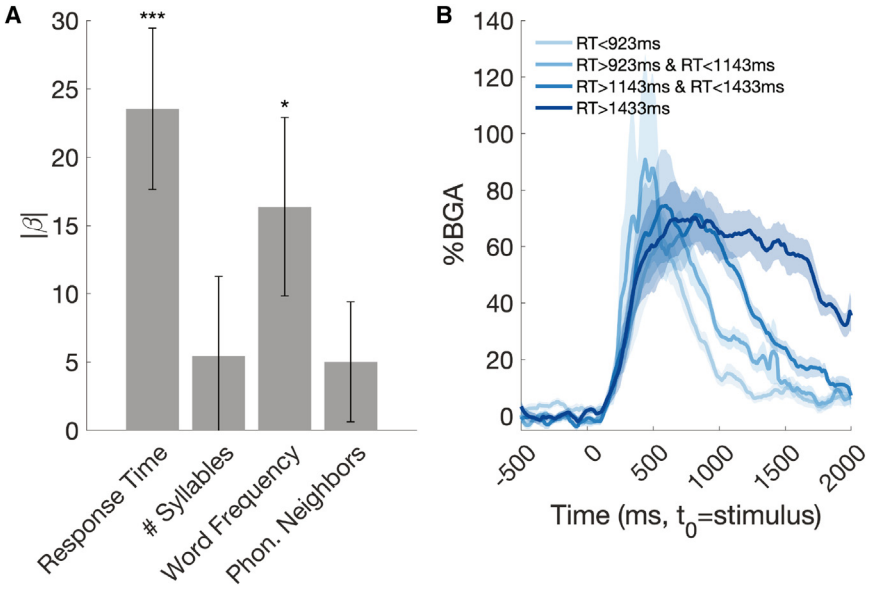

Figure 6. Functional broadband gamma activity in SMA for both scrambled and coherent picture naming conditions

(A) Linear mixed-effects modeling of pre-articulatory BGA (300–600 ms post-stimulus onset) in the coherent naming trials as a function of four features: RT, number of syllables, word frequency, and phonological neighborhood. ***$p < 0.001$, *$p < 0.05$.

(B) SMA BGA traces (mean ± SE) split by RT quartiles.

well as evidence from previous studies. First, IFS was active throughout articulation rather than only in the pre-articulation window, in contrast to SMA complex (Video S1; Figure 4B). Second, although IFS preceded SMA complex in its time to peak amplitude (Table 1; Figure 4B), it lagged SMA complex in its ability to predict RT (Figure 4D), and we interpreted RT prediction as the most meaningful feature in defining speech initiation regions. Lastly, previous work has suggested that IFS is part of a speech planning network that buffers sounds in verbal working memory for upcoming utterances.[8,26] Our results are concordant with this hypothesis. IFS was the only region with a biphasic BGA profile (Figure 4B). The first, early phase of activity could be the start of the buffering process for upcoming syllables. A tantalizing possibility is that the second phase of activity, which starts around 250 ms after speech onset and peaks 400 ms after speech onset, was driven by the second syllable in "scrambled." Future intracranial studies leveraging sEEG depth probes will help clarify IFS's activity time course in multi-word utterances. IFS, like SMA complex, has remained undercharacterized in iEEG but will likely receive more attention with the modern neurosurgical preference for sEEG over SDE in epilepsy monitoring.

Limitations of the study

It is possible that the high-gamma LFP signal is not sufficiently resolved to expose syllabic or phonemic activity and that smaller neural populations are tuned to these shorter motor commands. It is also worth considering that the BGA signal that we observed may not be speech specific; pre-articulation BGA contributes to the *Bereitschaftspotential*, or readiness potential,[1,13] observed in human EEG prior to internally generated movements, including speech.[50,77]

While the intracranial recordings in this study definitively show BGA in SMA during speech, we do not show that this set of SMA electrodes is speech specific as we did not control for the initiation of non-speech motor acts.

Our results revealed a heterogeneous set of functional profiles at electrodes in the SMA complex. We did not observe clearly differentiated functional responses between SMA and preSMA. This may have been due to poor sampling in preSMA specifically or across the medial wall more generally. Some researchers have argued that SMA and preSMA do not form functionally discrete areas in the first place; rather, they should be viewed as a continuum.[1] Future studies may leverage broader and denser iEEG coverage of the medial wall to clarify how the speech-related neural codes are organized along the preSMA-SMA axis.

Our results suggest that SMA is active primarily prior to articulation of a single word in a picture-naming task. Future studies should confirm whether the SMA is active primarily prior to phrase onset and before each word in a phrase. Our study concentrated on the most robust marker of single-unit activity (BGA), but other frequency bands should be inspected. We used LFP in our analyses to show that the SMA is active only at the word level. It is possible that some sub-populations, or even single units, in SMA are active during word articulation and mediate the release of individual phonemes.

RESOURCE AVAILABILITY

Lead contact

Further information and requests for resources should be directed to and will be fulfilled by the lead contact, Dr. Nitin Tandon (nitin.tandon@uth.tmc.edu).

Materials availability

This study did not generate new materials.

Data and code availability

- Deidentified data from the SMA electrodes have been deposited on OSF and are publicly available as of the date of publication at OSF: https://osf.io/7vs4d/.
- This paper does not report original code.
- Any additional information required to replicate the analyses reported in this paper is available from the lead contact upon request.

ACKNOWLEDGMENTS

We express our gratitude to all the patients who participated in this study, the neurologists at the Texas Comprehensive Epilepsy Program who participated in the care of these patients, and the nurses and technicians in the Epilepsy Monitoring Unit at Memorial Hermann Hospital who helped make this research

possible. This work was supported by the University of Texas System funding for the Texas Institute for Restorative Neurotechnologies.

AUTHOR CONTRIBUTIONS

Conceptualization, L.B., K.J.F., and N.T.; data curation, K.J.F. and P.S.R.; formal analysis and visualization, L.B. and O.W.; writing – original draft, L.B.; writing – review and editing, L.B., K.J.F., O.W., and N.T.; funding acquisition, N.T.; neurosurgical procedures, N.T.

DECLARATION OF INTERESTS

The authors declare no competing interests.

STAR★METHODS

Detailed methods are provided in the online version of this paper and include the following:

- KEY RESOURCES TABLE
- EXPERIMENTAL MODEL AND STUDY PARTICIPANT DETAILS
  - Human participants
- METHOD DETAILS
  - Experimental paradigm
  - Electrode implantation and data recording
  - Structural imaging and electrode localization
  - Analysis of audio recordings and phonetic forced alignment
  - Signal processing
- QUANTIFICATION AND STATISTICAL ANALYSIS
  - Brain-wide surface-based mixed-effects modeling
  - Regions of interest delineation
  - Regions of interest time features
  - Region of interest linear mixed effects modeling

SUPPLEMENTAL INFORMATION

Supplemental information can be found online at https://doi.org/10.1016/j.isci.2024.111531.

Received: May 22, 2024
Revised: September 18, 2024
Accepted: November 28, 2024
Published: December 4, 2024

REFERENCES

1. Nachev, P., Kennard, C., and Husain, M. (2008). Functional role of the supplementary and pre-supplementary motor areas. Nat. Rev. Neurosci. *9*, 856–869. https://doi.org/10.1038/nrn2478.
2. Alario, F.-X., Chainay, H., Lehericy, S., and Cohen, L. (2006). The role of the supplementary motor area (SMA) in word production. Brain Res. *1076*, 129–143. https://doi.org/10.1016/j.brainres.2005.11.104.
3. Jonas, S. (1981). The supplementary motor region and speech emission. J. Commun. Disord. *14*, 349–373. https://doi.org/10.1016/0021-9924(81)90019-8.
4. Krainik, A., Lehéricy, S., Duffau, H., Capelle, L., Chainay, H., Cornu, P., Cohen, L., Boch, A.-L., Mangin, J.-F., Le Bihan, D., and Marsault, C. (2003). Postoperative speech disorder after medial frontal surgery: role of the supplementary motor area. Neurology *60*, 587–594. https://doi.org/10.1212/01.wnl.0000048206.07837.59.
5. Penfield, W., and Welch, K. (1951). The supplementary motor area of the cerebral cortex; a clinical and experimental study. AMA. Arch. Neurol. Psychiatry *66*, 289–317. https://doi.org/10.1001/archneurpsyc.1951.02320090038004.
6. Lu, J., Zhao, Z., Zhang, J., Wu, B., Zhu, Y., Chang, E.F., Wu, J., Duffau, H., and Berger, M.S. (2021). Functional maps of direct electrical stimulation-induced speech arrest and anomia: a multicentre retrospective study. Brain *144*, 2541–2553. https://doi.org/10.1093/brain/awab125.
7. Laplane, D., Talairach, J., Meininger, V., Bancaud, J., and Orgogozo, J.M. (1977). Clinical consequences of corticectomies involving the supplementary motor area in man. J. Neurol. Sci. *34*, 301–314. https://doi.org/10.1016/0022-510x(77)90148-4.
8. Bohland, J.W., and Guenther, F.H. (2006). An fMRI investigation of syllable sequence production. Neuroimage *32*, 821–841. https://doi.org/10.1016/j.neuroimage.2006.04.173.
9. Brendel, B., Hertrich, I., Erb, M., Lindner, A., Riecker, A., Grodd, W., and Ackermann, H. (2010). The contribution of mesiofrontal cortex to the preparation and execution of repetitive syllable productions: An fMRI study. Neuroimage *50*, 1219–1230. https://doi.org/10.1016/j.neuroimage.2010.01.039.
10. Segawa, J.A., Tourville, J.A., Beal, D.S., and Guenther, F.H. (2015). The neural correlates of speech motor sequence learning. J. Cogn. Neurosci. *27*, 819–831. https://doi.org/10.1162/jocn_a_00737.
11. Simonyan, K., and Fuertinger, S. (2015). Speech networks at rest and in action: interactions between functional brain networks controlling speech production. J. Neurophysiol. *113*, 2967–2978. https://doi.org/10.1152/jn.00964.2014.
12. Goldenholz, D.M., Ahlfors, S.P., Hämäläinen, M.S., Sharon, D., Ishitobi, M., Vaina, L.M., and Stufflebeam, S.M. (2008). Mapping the signal-to-noise-ratios of cortical sources in magnetoencephalography and electroencephalography. Hum. Brain Mapp. *30*, 1077–1086. https://doi.org/10.1002/hbm.20571.
13. Deecke, L. (1987). Bereitschaftspotential as an indicator of movement preparation in supplementary motor area and motor cortex. Ciba Found. Symp. *132*, 231–250. https://doi.org/10.1002/9780470513545.ch14.
14. Chartier, J., Anumanchipalli, G.K., Johnson, K., and Chang, E.F. (2018). Encoding of Articulatory Kinematic Trajectories in Human Speech Sensorimotor Cortex. Neuron *98*, 1042–1054.e4. https://doi.org/10.1016/j.neuron.2018.04.031.
15. Conant, D., Bouchard, K.E., and Chang, E.F. (2014). Speech map in the human ventral sensory-motor cortex. Curr. Opin. Neurobiol. *24*, 63–67. https://doi.org/10.1016/j.conb.2013.08.015.
16. Mugler, E.M., Tate, M.C., Livescu, K., Templer, J.W., Goldrick, M.A., and Slutzky, M.W. (2018). Differential Representation of Articulatory Gestures and Phonemes in Precentral and Inferior Frontal Gyri. J. Neurosci. *38*, 9803–9813. https://doi.org/10.1523/JNEUROSCI.1206-18.2018.
17. Castellucci, G.A., Kovach, C.K., Howard, M.A., Greenlee, J.D.W., and Long, M.A. (2022). A speech planning network for interactive language use. Nature *602*, 117–122. https://doi.org/10.1038/s41586-021-04270-z.
18. Conner, C.R., Kadipasaoglu, C.M., Shouval, H.Z., Hickok, G., and Tandon, N. (2019). Network dynamics of Broca's area during word selection. PLoS One *14*, e0225756. https://doi.org/10.1371/journal.pone.0225756.
19. Forseth, K.J., Kadipasaoglu, C.M., Conner, C.R., Hickok, G., Knight, R.T., and Tandon, N. (2018). A lexical semantic hub for heteromodal naming in middle fusiform gyrus. Brain *141*, 2112–2126. https://doi.org/10.1093/brain/awy120.
20. Woolnough, O., Donos, C., Curtis, A., Rollo, P.S., Roccaforte, Z.J., Dehaene, S., Fischer-Baum, S., and Tandon, N. (2022). A Spatiotemporal Map of Reading Aloud. J. Neurosci. *42*, 5438–5450. https://doi.org/10.1523/JNEUROSCI.2324-21.2022.
21. Kermadi, I., Liu, Y., Tempini, A., and Rouiller, E.M. (1997). Effects of reversible inactivation of the supplementary motor area (SMA) on unimanual grasp and bimanual pull and grasp performance in monkeys. Somatosens. Mot. Res. *14*, 268–280. https://doi.org/10.1080/08990229770980.
22. Shima, K., and Tanji, J. (2000). Neuronal Activity in the Supplementary and Presupplementary Motor Areas for Temporal Organization of Multiple Movements. J. Neurophysiol. *84*, 2148–2160. https://doi.org/10.1152/jn.2000.84.4.2148.

23. Tanji, J., and Shima, K. (1994). Role for supplementary motor area cells in planning several movements ahead. Nature *371*, 413–416. https://doi.org/10.1038/371413a0.

24. Catani, M., Dell'Acqua, F., Vergani, F., Malik, F., Hodge, H., Roy, P., Valabregue, R., and Thiebaut de Schotten, M. (2012). Short frontal lobe connections of the human brain. Cortex *48*, 273–291. https://doi.org/10.1016/j.cortex.2011.12.001.

25. Dick, A.S., Garic, D., Graziano, P., and Tremblay, P. (2019). The frontal aslant tract (FAT) and its role in speech, language and executive function. Cortex *111*, 148–163. https://doi.org/10.1016/j.cortex.2018.10.015.

26. Guenther, F.H. (2016). Neural Control of Speech (MIT Press), pp. 103–106.

27. Forseth, K.J., Pitkow, X., Fischer-Baum, S., and Tandon, N. (2021). What The Brain Does As We Speak. Preprint at bioRxiv. https://doi.org/10.1101/2021.02.05.429841.

28. Snodgrass, J.G., and Vanderwart, M. (1980). A standardized set of 260 pictures: Norms for name agreement, image agreement, familiarity, and visual complexity. J. Exp. Psychol. Hum. Learn. *6*, 174–215. https://doi.org/10.1037/0278-7393.6.2.174.

29. Bernabei, J.M., Arnold, T.C., Shah, P., Revell, A., Ong, I.Z., Kini, L.G., Stein, J.M., Shinohara, R.T., Lucas, T.H., Davis, K.A., et al. (2021). Electrocorticography and stereo EEG provide distinct measures of brain connectivity: implications for network models. Brain Commun. *3*, fcab156. https://doi.org/10.1093/braincomms/fcab156.

30. Tandon, N., Tong, B.A., Friedman, E.R., Johnson, J.A., Von Allmen, G., Thomas, M.S., Hope, O.A., Kalamangalam, G.P., Slater, J.D., and Thompson, S.A. (2019). Analysis of Morbidity and Outcomes Associated With Use of Subdural Grids vs Stereoelectroencephalography in Patients With Intractable Epilepsy. JAMA Neurol. *76*, 672–681. https://doi.org/10.1001/jamaneurol.2019.0098.

31. Allen, M., Poggiali, D., Whitaker, K., Marshall, T.R., van Langen, J., and Kievit, R.A. (2019). Raincloud plots: a multi-platform tool for robust data visualization [version 2; peer review: 2 approved]. Wellcome Open Res. *4*, 63. https://doi.org/10.12688/wellcomeopenres.15191.2.

32. McAuliffe, M., Socolof, M., Mihuc, S., Wagner, M., and Sonderegger, M. (2017). Montreal Forced Aligner: Trainable Text-Speech Alignment Using Kaldi. In Interspeech 2017 (ISCA), pp. 498–502. https://doi.org/10.21437/Interspeech.2017-1386.

33. Hayes, B. (2011). Introductory Phonology (John Wiley & Sons), p. 15.

34. Conner, C.R., Ellmore, T.M., Pieters, T.A., DiSano, M.A., and Tandon, N. (2011). Variability of the Relationship between Electrophysiology and BOLD-fMRI across Cortical Regions in Humans. J. Neurosci. *31*, 12855–12865. https://doi.org/10.1523/JNEUROSCI.1457-11.2011.

35. Kadipasaoglu, C.M., Baboyan, V.G., Conner, C.R., Chen, G., Saad, Z.S., and Tandon, N. (2014). Surface-based mixed effects multilevel analysis of grouped human electrocorticography. Neuroimage *101*, 215–224. https://doi.org/10.1016/j.neuroimage.2014.07.006.

36. Crone, N.E., Sinai, A., and Korzeniewska, A. (2006). High-frequency gamma oscillations and human brain mapping with electrocorticography. Prog. Brain Res. *159*, 275–295. https://doi.org/10.1016/S0079-6123(06)59019-3.

37. Nir, Y., Fisch, L., Mukamel, R., Gelbard-Sagiv, H., Arieli, A., Fried, I., and Malach, R. (2007). Coupling between Neuronal Firing Rate, Gamma LFP, and BOLD fMRI Is Related to Interneuronal Correlations. Curr. Biol. *17*, 1275–1285. https://doi.org/10.1016/j.cub.2007.06.066.

38. Bouchard, K.E., Mesgarani, N., Johnson, K., and Chang, E.F. (2013). Functional organization of human sensorimotor cortex for speech articulation. Nature *495*, 327–332. https://doi.org/10.1038/nature11911.

39. Forseth, K.J., Hickok, G., Rollo, P.S., and Tandon, N. (2020). Language prediction mechanisms in human auditory cortex. Nat. Commun. *11*, 5240. https://doi.org/10.1038/s41467-020-19010-6.

40. Hickok, G. (2012). Computational neuroanatomy of speech production. Nat. Rev. Neurosci. *13*, 135–145. https://doi.org/10.1038/nrn3158.

41. Gajardo-Vidal, A., Lorca-Puls, D.L., Team, P., Warner, H., Pshdary, B., Crinion, J.T., Leff, A.P., Hope, T.M.H., Geva, S., Seghier, M.L., et al. (2021). Damage to Broca's area does not contribute to long-term speech production outcome after stroke. Brain *144*, 817–832. https://doi.org/10.1093/brain/awaa460.

42. Mandonnet, E., and Duffau, H. (2021). Broca's area: why was neurosurgery neglected for so long when seeking to re-establish the scientific truth? Brain *144*, e60. https://doi.org/10.1093/brain/awab195.

43. Suarez-Meade, P., Marenco-Hillembrand, L., Sabsevitz, D., Okromelidze, L., Blake Perdikis, B.S., Sherman, W.J., Quinones-Hinojosa, A., Middlebrooks, E.H., and Chaichana, K.L. (2022). Surgical resection of gliomas in the dominant inferior frontal gyrus: Consecutive case series and anatomy review of Broca's area. Clin. Neurol. Neurosurg. *223*, 107512. https://doi.org/10.1016/j.clineuro.2022.107512.

44. Willett, F.R., Kunz, E.M., Fan, C., Avansino, D.T., Wilson, G.H., Choi, E.Y., Kamdar, F., Glasser, M.F., Hochberg, L.R., Druckmann, S., et al. (2023). A high-performance speech neuroprosthesis. Nature *620*, 1031–1036. https://doi.org/10.1038/s41586-023-06377-x.

45. Hertrich, I., Dietrich, S., and Ackermann, H. (2016). The role of the supplementary motor area for speech and language processing. Neurosci. Biobehav. Rev. *68*, 602–610. https://doi.org/10.1016/j.neubiorev.2016.06.030.

46. Ikeda, A., Lüders, H.O., Burgess, R.C., and Shibasaki, H. (1992). Movement-related potentials recorded from supplementary motor area and primary motor area: role of supplementary motor area in voluntary movements. Brain *115*, 1017–1043. https://doi.org/10.1093/brain/115.4.1017.

47. Ohara, S., Ikeda, A., Kunieda, T., Yazawa, S., Baba, K., Nagamine, T., Taki, W., Hashimoto, N., Mihara, T., and Shibasaki, H. (2000). Movement-related change of electrocorticographic activity in human supplementary motor area proper. Brain *123*, 1203–1215. https://doi.org/10.1093/brain/123.6.1203.

48. Ziegler, W., Kilian, B., and Deger, K. (1997). The role of the left mesial frontal cortex in fluent speech: Evidence from a case of left supplementary motor area hemorrhage. Neuropsychologia *35*, 1197–1208. https://doi.org/10.1016/S0028-3932(97)00040-7.

49. Deecke, L., Kornhuber, H.H., Lang, W., Lang, M., and Schreiber, H. (1985). Timing function of the frontal cortex in sequential motor and learning tasks. Hum. Neurobiol. *4*, 143–154.

50. Grözinger, B., Kornhuber, H.H., Kriebel, J., Szirtes, J., and Westphal, K.T.P. (1980). The Bereitschaftspotential Preceding the Act of Speaking. Also an Analysis of Artifacts. In Progress in Brain Research, H.H. Kornhubek and L. Deecke, eds. (Elsevier), pp. 798–804. https://doi.org/10.1016/S0079-6123(08)61705-7.

51. Hickok, G., Venezia, J.H., and Teghipco, A. (2021). Beyond Broca: Neural Architecture and Evolution of a Dual Motor Speech Coordination System. Preprint at PsyArXiv. https://doi.org/10.31234/osf.io/tewna.

52. Merchant, H., Zarco, W., Pérez, O., Prado, L., and Bartolo, R. (2011). Measuring time with different neural chronometers during a synchronization-continuation task. Proc. Natl. Acad. Sci. USA *108*, 19784–19789. https://doi.org/10.1073/pnas.1112933108.

53. Merchant, H., Pérez, O., Zarco, W., and Gámez, J. (2013). Interval Tuning in the Primate Medial Premotor Cortex as a General Timing Mechanism. J. Neurosci. *33*, 9082–9096. https://doi.org/10.1523/JNEUROSCI.5513-12.2013.

54. Cadena-Valencia, J., García-Garibay, O., Merchant, H., Jazayeri, M., and Lafuente, V. de (2018). Entrainment and maintenance of an internal metronome in supplementary motor area. Elife *7*, e38983. https://doi.org/10.7554/eLife.38983.

55. Ghazanfar, A.A., and Poeppel, D. (2014). The neurophysiology and evolution of the speech rhythm. In The cognitive neurosciences, 5th ed, M.S. Gazzaniga and G.R. Mangun, eds. (MIT Press), pp. 629–638.

56. ten Oever, S., and Martin, A.E. (2021). An oscillating computational model can track pseudo-rhythmic speech by using linguistic predictions. Elife *10*, e68066. https://doi.org/10.7554/eLife.68066.

57. Bohland, J.W., Bullock, D., and Guenther, F.H. (2010). Neural representations and mechanisms for the performance of simple speech sequences. J. Cogn. Neurosci. *22*, 1504–1529. https://doi.org/10.1162/jocn.2009.21306.

58. Guenther, F.H., Ghosh, S.S., and Tourville, J.A. (2006). Neural modeling and imaging of the cortical interactions underlying syllable production. Brain Lang. *96*, 280–301. https://doi.org/10.1016/j.bandl.2005.06.001.

59. Chang, S.-E., and Guenther, F.H. (2019). Involvement of the Cortico-Basal Ganglia-Thalamocortical Loop in Developmental Stuttering. Front. Psychol. *10*, 3088. https://doi.org/10.3389/fpsyg.2019.03088.

60. Ruan, J., Bludau, S., Palomero-Gallagher, N., Caspers, S., Mohlberg, H., Eickhoff, S.B., Seitz, R.J., and Amunts, K. (2018). Cytoarchitecture, probability maps, and functions of the human supplementary and pre-supplementary motor areas. Brain Struct. Funct. *223*, 4169–4186. https://doi.org/10.1007/s00429-018-1738-6.

61. Lee, K.M., Chang, K.H., and Roh, J.K. (1999). Subregions within the supplementary motor area activated at different stages of movement preparation and execution. Neuroimage *9*, 117–123. https://doi.org/10.1006/nimg.1998.0393.

62. Alm, P.A. (2004). Stuttering and the basal ganglia circuits: a critical review of possible relations. J. Commun. Disord. *37*, 325–369. https://doi.org/10.1016/j.jcomdis.2004.03.001.

63. Chang, S.-E., and Zhu, D.C. (2013). Neural network connectivity differences in children who stutter. Brain *136*, 3709–3726. https://doi.org/10.1093/brain/awt275.

64. Josephs, K.A., Duffy, J.R., Strand, E.A., Machulda, M.M., Senjem, M.L., Master, A.V., Lowe, V.J., Jack, C.R., and Whitwell, J.L. (2012). Characterizing a neurodegenerative syndrome: primary progressive apraxia of speech. Brain *135*, 1522–1536. https://doi.org/10.1093/brain/aws032.

65. Utianski, R.L., Duffy, J.R., Clark, H.M., Strand, E.A., Botha, H., Schwarz, C.G., Machulda, M.M., Senjem, M.L., Spychalla, A.J., Jack, C.R., et al. (2018). Prosodic and Phonetic Subtypes of Primary Progressive Apraxia of Speech. Brain Lang. *184*, 54–65. https://doi.org/10.1016/j.bandl.2018.06.004.

66. Ardila, A. (2020). Supplementary motor area aphasia revisited. J. Neurolinguistics *54*, 100888. https://doi.org/10.1016/j.jneuroling.2020.100888.

67. Pinson, H., Van Lerbeirghe, J., Vanhauwaert, D., Van Damme, O., Hallaert, G., and Kalala, J.-P. (2022). The supplementary motor area syndrome: a neurosurgical review. Neurosurg. Rev. *45*, 81–90. https://doi.org/10.1007/s10143-021-01566-6.

68. Berthier, M., Dávila, G., Moreno-Torres, I., Beltrán-Corbellini, Á., Santana-Moreno, D., Torres-Prioris, M.J., Massone, M.I., Cruces, R., Roé Vellvé, N., and Thurnhofer-Hemsi, K. (2015). Loss of regional accent after damage to the speech production network. Front. Hum. Neurosci. *9*, 610.

69. Busan, P. (2020). Developmental stuttering and the role of the supplementary motor cortex. J. Fluency Disord. *64*, 105763. https://doi.org/10.1016/j.jfludis.2020.105763.

70. Nakajima, R., Kinoshita, M., Yahata, T., and Nakada, M. (2020). Recovery time from supplementary motor area syndrome: relationship to postoperative day 7 paralysis and damage of the cingulum. J. Neurosurg. *132*, 865–874. https://doi.org/10.3171/2018.10.JNS182391.

71. Zentner, J., Hufnagel, A., Pechstein, U., Wolf, H.K., and Schramm, J. (1996). Functional results after resective procedures involving the supplementary motor area. J. Neurosurg. *85*, 542–549. https://doi.org/10.3171/jns.1996.85.4.0542.

72. Sajid, N., Parr, T., Hope, T.M., Price, C.J., and Friston, K.J. (2020). Degeneracy and Redundancy in Active Inference. Cereb. Cortex *30*, 5750–5766. https://doi.org/10.1093/cercor/bhaa148.

73. Sailor, J., Meyerand, M.E., Moritz, C.H., Fine, J., Nelson, L., Badie, B., and Haughton, V.M. (2003). Supplementary Motor Area Activation in Patients with Frontal Lobe Tumors and Arteriovenous Malformations. AJNR Am J Neuroradiol. *6*, 1837–1842.

74. Park, C.H., Chang, W.H., Lee, M., Kwon, G.H., Kim, L., Kim, S.T., and Kim, Y.-H. (2015). Which motor cortical region best predicts imagined movement? Neuroimage *113*, 101–110. https://doi.org/10.1016/j.neuroimage.2015.03.033.

75. Roland, P.E., Larsen, B., Lassen, N.A., and Skinhøj, E. (1980). Supplementary motor area and other cortical areas in organization of voluntary movements in man. J. Neurophysiol. *43*, 118–136. https://doi.org/10.1152/jn.1980.43.1.118.

76. Moses, D.A., Leonard, M.K., Makin, J.G., and Chang, E.F. (2019). Real-time decoding of question-and-answer speech dialogue using human cortical activity. Nat. Commun. *10*, 3096. https://doi.org/10.1038/s41467-019-10994-4.

77. McArdle, J.J., Mari, Z., Pursley, R.H., Schulz, G.M., and Braun, A.R. (2009). Electrophysiological evidence of functional integration between the language and motor systems in the brain: A study of the speech Bereitschaftspotential. Clin. Neurophysiol. *120*, 275–284. https://doi.org/10.1016/j.clinph.2008.10.159.

78. Dale, A.M., Fischl, B., and Sereno, M.I. (1999). Cortical surface-based analysis. I. Segmentation and surface reconstruction. Neuroimage *9*, 179–194. https://doi.org/10.1006/nimg.1998.0395.

79. Cox, R.W. (1996). AFNI: software for analysis and visualization of functional magnetic resonance neuroimages. Comput. Biomed. Res. *29*, 162–173. https://doi.org/10.1006/cbmr.1996.0014.

80. Conner, C.R., Chen, G., Pieters, T.A., and Tandon, N. (2014). Category Specific Spatial Dissociations of Parallel Processes Underlying Visual Naming. Cereb. Cortex *24*, 2741–2750. https://doi.org/10.1093/cercor/bht130.

81. Woolnough, O., Forseth, K.J., Rollo, P.S., and Tandon, N. (2019). Uncovering the functional anatomy of the human insula during speech. Elife *8*, e53086. https://doi.org/10.7554/eLife.53086.

82. Tandon, N., and Luders, H. (2008). Cortical mapping by electrical stimulation of subdural electrodes: language areas. In Textbook of Epilepsy Surgery, H.O. Luders, ed. (McGraw Hill), pp. 1001–1015.

83. Gonzalez-Martinez, J., Mullin, J., Vadera, S., Bulacio, J., Hughes, G., Jones, S., Enatsu, R., and Najm, I. (2014). Stereotactic placement of depth electrodes in medically intractable epilepsy: Technical note. J. Neurosurg. *120*, 639–644. https://doi.org/10.3171/2013.11.JNS13635.

84. González-Martínez, J., Bulacio, J., Thompson, S., Gale, J., Smithason, S., Najm, I., and Bingaman, W. (2016). Technique, Results, and Complications Related to Robot-Assisted Stereoelectroencephalography. Neurosurgery *78*, 169–180. https://doi.org/10.1227/NEU.0000000000001034.

85. Rollo, P.S., Rollo, M.J., Zhu, P., Woolnough, O., and Tandon, N. (2021). Oblique trajectory angles in robotic stereo-electroencephalography. J. Neurosurg. *135*, 245–254. https://doi.org/10.3171/2020.5.JNS20975.

86. Pieters, T.A., Conner, C.R., and Tandon, N. (2013). Recursive grid partitioning on a cortical surface model: an optimized technique for the localization of implanted subdural electrodes. J. Neurosurg. *118*, 1086–1097. https://doi.org/10.3171/2013.2.JNS121450.

87. Boersma, P., and Weenink, D. (2007). PRAAT: Doing phonetics by computer (Version 5.3.51).

88. Bořil, T., and Skarnitzl, R. (2016). Tools rPraat and mPraat. In Text, Speech, and Dialogue Lecture Notes in Computer Science, P. Sojka, A. Horák, I. Kopeček, and K. Pala, eds. (Springer International Publishing), pp. 367–374. https://doi.org/10.1007/978-3-319-45510-5_42.

89. Kadipasaoglu, C.M., Forseth, K., Whaley, M., Conner, C.R., Rollo, M.J., Baboyan, V.G., and Tandon, N. (2015). Development of grouped icEEG for the study of cognitive processing. Front. Psychol. *6*, 1008.

90. Woolnough, O., Rollo, P.S., Forseth, K.J., Kadipasaoglu, C.M., Ekstrom, A.D., and Tandon, N. (2020). Category Selectivity for Face and Scene

Recognition in Human Medial Parietal Cortex. Curr. Biol. *30*, 2707–2715.e3. https://doi.org/10.1016/j.cub.2020.05.018.

91. McCarty, M.J., Woolnough, O., Mosher, J.C., Seymour, J., and Tandon, N. (2022). The Listening Zone of Human Electrocorticographic Field Potential Recordings. eNeuro *9*, ENEURO.0492-21.2022. https://doi.org/10.1523/ENEURO.0492-21.2022.

92. Chen, G., Saad, Z.S., Nath, A.R., Beauchamp, M.S., and Cox, R.W. (2012). FMRI group analysis combining effect estimates and their variances. Neuroimage *60*, 747–765. https://doi.org/10.1016/j.neuroimage.2011.12.060.

93. Destrieux, C., FISCHL, B., DALE, A., and HALGREN, E. (2010). Automatic parcellation of human cortical gyri and sulci using standard anatomical nomenclature. Neuroimage *53*, 1–15. https://doi.org/10.1016/j.neuroimage.2010.06.010.

94. Kim, J.-H., Lee, J.-M., Jo, H.J., Kim, S.H., Lee, J.H., Kim, S.T., Seo, S.W., Cox, R.W., Na, D.L., Kim, S.I., and Saad, Z.S. (2010). Defining functional SMA and pre-SMA subregions in human MFC using resting state fMRI: functional connectivity-based parcellation method. Neuroimage *49*, 2375–2386. https://doi.org/10.1016/j.neuroimage.2009.10.016.

95. Vaden, K.I., Halpin, H.R., and Hickok, G. (2009). Irvine Phonotactic Online Dictionary, Version 2.0.

STAR★METHODS

KEY RESOURCES TABLE

REAGENT or RESOURCE	SOURCE	IDENTIFIER
Software and algorithms		
MATLAB 2021	MathWorks, MA, USA	https://www.mathworks.com/
Freesurfer	Dale et al.[78]	http://freesurfer.net
AFNI/SUMA	Cox[79]	https://afni.nimh.nih.gov
Python v2.7	N/A	www.python.org
Deposited data		
Preprocessed data	This paper	OSF: https://osf.io/7vs4d/
Other		
ECoG and SEEG electrodes	PMT Corporation	http://pmtcorp.com
Neurofax EEG System	Nihon Kohden	www.nihonkohden.com
Blackrock NeuroPort Acquisition System	BlackRock Microsystems, UT, USA	https://www.blackrockmicro.com
Robotic Surgical Assistant (ROSA)	Medtech, Montpellier, France	https://www.medtech.fr
Lavalier microphone AT898	Audio Technica	www.audio-technica.com

EXPERIMENTAL MODEL AND STUDY PARTICIPANT DETAILS

Human participants

We enrolled 115 patients (54 men, 61 women; mean age 33 ± 10 years; mean IQ 96 ± 14, 10 left-handed) with intractable epilepsy undergoing monitoring with intracranial electrodes.[27] Eight patients were each implanted twice, and one patient was implanted three times, for a total of 125 subject sessions. The study design was approved by the committee for the protection of human subjects at The University of Texas Health Science Center as Protocol Number HSC-MS-06-0385. Nine additional patients recorded from were excluded from analysis as they were determined to be right hemisphere-dominant for language.

METHOD DETAILS

Experimental paradigm

Subjects engaged in a picture naming task.[19,27,80,81] They were instructed to articulate the name of common objects depicted by line drawings[28] as quickly and accurately as possible. A control condition was intermixed consisting of the same images with pixel blocks randomly rotated; for these trials, subjects were instructed to respond with "scrambled." Each visual stimulus was displayed for 2 s on a 15-inch LCD screen positioned at eye level, with an interstimulus interval of 4 s with a uniformly distributed jitter of ±500 ms. A minimum of 120 (mean 298) visual stimuli were presented to each subject using stimulus presentation software (Python v2.7). 82 ± 21 (mean ± SD; range: 31–125) scrambled trials were presented per subject. In total, the word 'scrambled' was correctly produced 10,788 times across the cohort.

Electrode implantation and data recording

Subdural grid electrodes (SDEs; n = 39 implants) – subdural platinum-iridium electrodes embedded in a silicone elastomer sheet (PMT Corporation, top-hat design; 3-mm diameter cortical contact) – were surgically implanted via a craniotomy.[82] Electrocorticography recordings were performed at least 2 days after the craniotomy. Stereo-electroencephalography (sEEG; n = 86 implants) probes contained platinum-iridium electrode contacts (PMT Corporation; 0.8-mm diameter, 2.0-mm length cylinders; separated from adjacent contacts by 1.5–2.43 mm), and were implanted using the Robotic Surgical Assistant (ROSA, Zimmer-Biomet), with stereotactic skull screws registered to both a computed tomographic angiogram and an anatomical MRI.[30,83–85] There were 8–16 recording contacts along each depth probe, and each patient had multiple (12–20) probes implanted. Intracranial EEG data were collected with a sampling rate of 1 kHz and bandwidth of 0.15–300 Hz using Neurofax (Nihon Kohden) or with a sampling rate of 2 kHz and bandwidth of 0.1–700 Hz using NeuroPort NSP (Blackrock Microsystems). Continuous audio recordings were performed with both an omnidirectional microphone (Audio Technica U841A, 30 to 20,000 Hz response, 73 dB SNR) placed adjacent to the presentation laptop and a cardioid lavalier microphone (Audio Technica AT898, 200 to 15,000 Hz response, 63 dB SNR) clipped to clothing near the mouth. These recordings were analyzed offline to transcribe subject responses, as well as to determine the time of articulatory onset and offset.

We used the term 'electrode' to refer to a single recording contact along an sEEG probe or ECoG strip. 22,334 electrodes were implanted in total. We excluded electrodes with movement artifacts, electrical noise, or epileptic activity. Each electrode was then re-referenced to the common average of all remaining electrode.

Structural imaging and electrode localization

Preoperative anatomical MRI scans were obtained using a 3T whole-body MRI scanner (Philips Medical Systems) fitted with a 16-channel SENSE head coil. Images were collected using a magnetization-prepared 180° radiofrequency pulse and rapid gradient-echo sequence with 1-mm sagittal slices and an in-plane resolution of 0.938 × 0.938 mm. Pial surface reconstructions were computed with FreeSurfer (v5.1)[78] and imported to AFNI.[79] Postoperative CT scans were registered to preoperative MRI scans for localization of electrodes relative to cortex. Grid electrode locations were determined by a recursive grid partitioning technique and then optimized using intraoperative photographs.[86] Depth electrode locations were informed by implantation trajectories from the ROSA system. Electrode locations were projected onto a FreeSurfer-generated cortical pial surface. These locations were then transformed to standard population cortical space with a nonlinear surface-based registration. Both brain-wide analyses and ROI analyses were completed in this standard space.

Analysis of audio recordings and phonetic forced alignment

Audio recordings were used to annotate behavioral timepoints in trials. Speech onset was defined as the first acoustic signature of speech. For 'scrambled', we labeled the first timepoint where a high-frequency (3+ kHz) broadband power increase—typical sibilants like/s/—was visible. To determine variability within and across subjects' articulations, we used the Montreal Forced Aligner (MFA) to force-align all of the phones of 'scrambled' with their acoustic signatures in every trial.[32] Single-trial recordings were extracted and saved as separate wav files. MFA was then run using default parameters. MFA outputs Praat TextGrids,[87] which were read back into MATLAB using the mPraat toolbox.[88]

Signal processing

Line noise was removed from the raw electrocorticography local field potential with zero-phase second-order Butterworth bandstop filters at 60, 120, and 180 Hz. Broadband high-gamma activity (BGA; 70 to 150 Hz) was then extracted by a) bandpass filtering with a frequency-domain Hilbert filter (paired sigmoid flanks with half-width 1.5 Hz) and b) calculating power in the resulting analytic signal. All analyses were performed with trials time-locked to either picture presentation or to articulation onset. Baseline was defined relative to the picture presentation (−500 to −100 ms). BGA traces were smoothed for plotting with a third-order, 251 frame length Savitzky-Golay finite impulse response filter.

QUANTIFICATION AND STATISTICAL ANALYSIS

Brain-wide surface-based mixed-effects modeling

For whole-brain analyses, estimates of cortical BGA at every vertex on the surface in both hemispheres were estimated using surface-based mixed-effects multilevel analysis[19,34,35,78,89] (SB-MEMA). Refer to Kadipasaoglu et al.[35] for a complete description of the SB-MEMA and to Forseth et al.[19] and Woolnough et al.[90] for previous applications of the method. Briefly, SB-MEMA generates statistically robust and topologically precise estimates of BGA using geodesic activation spread from recording electrodes.[35,91] SB-MEMA accounts for outliers by weighting electrodes by their trial-to-trial variance estimates[92] and accounts for the sparse sampling problem in iEEG by correcting for sampling imbalances between regions. SB-MEMA maps of cortical activation were thresholded at 15% change from baseline. SB-MEMA movies were generated by re-running the SB-MEMA analysis with 150 ms windows and a 10 ms time stride. Frames were then spatially smoothed with a Gaussian smoothing filter (2 mm FWHM).

Regions of interest delineation

Left-hemisphere regions of interest were determined based on the Destrieux Atlas[93] and prior intracranial electrode studies,[20,27] resulting in an anatomically-functionally defined set of ROIs. The delineated ROIs rely on the Destrieux Atlas to parcellate the suprasylvian speech production network. The following regions were defined from this atlas: inferior frontal sulcus (IFS), pars triangularis (parsTri), pars opercularis (parsOp), precentral sulcus (preCS), pre- and postcentral gyrus (preCG and postCG), subcentral gyrus (SCG), central sulcus (CS), Heschl's gyrus (HG) and planum temporale (PT). Supplementary motor area (SMA), and preSMA were defined using geodesic radii around a defined center point, based on prior studies.[20,27] The boundary between SMA and preSMA was approximated with a vertical plane extending from the anterior commissure.[94] Centroids of these ROIs, in Talairach space, were: SMA -4, −5, 51; preSMA −4, 17, 38. All SMA and preSMA electrode assignments were validated manually based on each subject's native cortical surface.

ROI boundaries on the pial surface were used to identify electrodes within an ROI; if an electrode was localized to a vertex within the ROI, it was considered part of the ROI. 1,479 electrodes from 98 subjects were localized within the ROIs. Active electrodes were electrodes whose trial-averaged BGA percent change exceeded 20% increase from baseline in a peri-articulatory window from −500 to 500 ms relative to articulation onset. Inactive electrodes were excluded from further analysis. 631 ROI electrodes from 81 subjects were active above baseline.

Regions of interest time features

Timepoints of significant activation within an ROI were identified using mixed-effects models (i.e., BGA ~1 + (1 | Subject) + (1 | Subject:Electrode)) using all trials and all electrodes with the ROI, testing at each 10 ms resolution with a Benjamini-Hochberg false discovery rate correction ($q < 0.05$).

To quantify timing differences across ROIs, we used a bootstrapping approach to estimate time features and their confidence intervals. We generated bootstrap distributions for each ROI by randomly sampling trials with replacement within each electrode before averaging within, and then across, subjects, repeated 1000 times. We calculated median and 95% confidence intervals for two timing features. These features were: (1) the time point at which trial-averaged BGA reached its peak amplitude ('Time to Peak Amp'), and (2) the first time point at which trial-averaged BGA exceeded 3.5 standard deviations of the baseline to reflect 0.001 significance ('Time to First Amp>Baseline').

Region of interest linear mixed effects modeling

Linear mixed effects (LME) models were used to model BGA as a function of response time (RT) in each ROI. All modeling was performed in MATLAB using the fitlme() function. RT was modeled as a function of BGA, as a fixed effect, with a random effect of electrode, nested within subject. In Wilkinson notation, the model formula was: BGA ~ RT + (1 | Subject) + (1 | Subject:Electrode). Independent LMEs were fit at each time point in each ROI. Positive beta values indicate BGA increases with shorter RTs. Time points with significant betas were identified across the time course with a Benjamini-Hochberg FDR-corrected threshold at $q = 0.05$.

We also used LMEs in the coherent picture naming condition to model the relationship between BGA and four predictor variables: response time and number of syllables, phonological neighborhood, and word frequency, all sourced from the Irvine Phonotactic Online Dictionary.[95] The model formula was: BGA ~ RT + # Syllables + Word frequency + Phonological neighborhood + (1 | Subject) + (1 | Subject:Electrode).